High-resolution Beijing MST radar detection of tropopause structure and

variability over Xianghe (39.75° N, 116.96° E), China

Feilong Chen[1,2], Gang Chen[1*], Yufang Tian[3], Shaodong Zhang[1], Kaiming Huang[1],

Chen Wu[1], Weifan Zhang[1]

[1]School of Electronic Information, Wuhan University, Wuhan 430072, China.

[2]School of Information Engineering, Nanchang Hangkong University, Nanchang

330063, China.

[3]Key Laboratory of Middle Atmosphere and Global Environment Observation, Institute

of Atmospheric Physics, Chinese Academy of Sciences, Beijing 100029, China.

*Corresponding author: Gang Chen (g.chen@whu.edu.cn)

Abstract.

As a result of partial specular reflection from the atmospheric stable layer, the radar

tropopause (RT) can simply and directly be detected by VHF radars with vertical

incidence. Here, the Beijing MST radar measurements are used to investigate the

structure and the variabilities of the tropopause in Xianghe, China with a temporal

resolution of 0.5 hour from November 2011 to May 2017. High-resolution radar-

derived tropopause is compared with the thermal lapse-rate tropopause (LRT) that

defined by the World Meteorological Organization (WMO) criterion from twice daily

radiosonde soundings and with the dynamical potential vorticity tropopause (PVT) that

defined as the height of 2 PVU surface. We only consider tropopauses below 16km in

this study because of limitations with the radar system. During all the seasons, the RT

and the LRT in altitude agree well with each other with a correlation coefficient of ≥ 0.74. Statistically, weaker (higher) tropopause sharpness seems to contribute to larger (smaller) difference between the RT and the LRT in altitude. The RT agrees well with the PVT in altitude during winter and spring with a correlation coefficient of ≥ 0.72, while the correlation coefficient in summer is only 0.33. As expected, the monthly mean RT and LRT height both show seasonal variations. Lomb-Scargle periodograms show that the tropopause exhibits obvious diurnal variation throughout the seasons, whereas the semidiurnal oscillations are rare and occasionally observed during summer and later spring. Our study shows the potential of the Beijing MST radar to determine the tropopause height, as well as present its diurnal oscillations.

Key words: VHF radar; MST radar; tropopause; diurnal oscillation.

1. Introduction

The tropopause marks a transition zone separating the well-mixed convectively active troposphere from the stably stratified and more quiescent stratosphere. Its structure and variability is characterized by large changes in thermal (e.g., lapse rate), dynamical (e.g., potential vorticity), and chemical properties (e.g., ozone and water vapor) and hence acts as a key role for the stratosphere-troposphere exchange (STE) processes (Hoinka, 1998; Seidel et l., 2001). The height of the tropopause depends significantly on the latitude, with about 17 km near the equator and less than 9-10 km at polar latitudes (Ramakrishnan, 1933). Over subtropical latitudes with the presence of subtropical jet, where the tropopause experiences rapid change or breaking,

46   tropopause folding events are commonly observed (Pan et al., 2004). Climatologically,

47   the altitude of the tropopause represents the seasonal variation of the flux of

48   stratospheric air intruding into the troposphere (Appenzeller et al., 1996). Moreover,

49   the tropopause height trends can be a sensitive indicator of anthropogenic climate

50   change (Sausen and Santer, 2003; Santer et al., 2003a; Añel et al., 2006).

51   A variety of ways are available to determine the extratropical tropopause.

52   Radiosonde sounding is the most commonly used to define the thermal tropopause

53   (hereafter referred to as LRT) based on temperature lapse-rate (WMO, 1957). The

54   thermal definition of tropopause can be applied globally and the tropopause height

55   easily be determined from one individual profile (Santer et al., 2003). Another feasible

56   definition is to use a specific potential vorticity (PV) surface to represent the dynamical

57   tropopause (hereafter referred to as PVT) (Reed, 1955; Hoskins et al., 1985).

58   Dynamical definition has the advantage that the PV is a conserved property (under

59   adiabatic and friction-less conditions) of an air mass (Hoskins et al., 1985; Bethan et

60   al., 1996). Values in the range 1-4 PVU (1 PVU=$10^6 \mathrm{m}^2 s^{-1} Kkg^{-1}$) are used in previous

61   researches in the Northern Hemisphere (e.g. Baray et al., 2000; Sprenger et al., 2003;

62   Hoerling et al., 1991). The threshold of 2 PVU surface is the most commonly used

63   (Gettelman et al., 2011). Dynamical definition, however, is not applicable near the

64   equator, where the PV tends to be 0 (e.g., Hoerling et al., 1991; Nielsen-Gammon et al.,

65   2001). Creating a blended tropopause globally may probably a good way forward

66   (Wilcox et al., 2011). In addition, the data of GPS radio occultation satellites is also an

67   effective way and commonly applied to study tropopause (e.g. Schmidt et al., 2005;

68   Son et al., 2011).

69   As a result of partial specular reflection from stable atmospheric layer, the radar

70   tropopause (RT) can be well represented and identified by atmospheric radars operating

71   at meter wavelength (VHF band) and directing at vertical incidence (Gage and Green,

72   1979). Research activity increased remarkably following the first report on VHF radar

73   detection of tropopause by Gage and Green (1979), for instance, the researches in

74   middle latitudes (e.g. Hermawan et al., 1998), polar regions (e.g. Hall, 2013a), and

75   tropical regions (e.g. Das et al., 2008; Ravindrababu et al., 2014). Several methods have

76   been proposed to determine the tropopause height via radar echo power, including the

77   largest gradient in echo power (Vaughan et al., 1995; Alexander et al., 2013), the

78   maximum echo power (Vaughan et al., 1995; Hall et al., 2009), and the specific value

79   of echo power (Gage and Green, 1982; Yamamoto et al., 2003). The method of the RT

80   height determination used in this paper will be described in detail in next section.

81   The biggest advantage of VHF radar measurements is the ability of continuous

82   operation unmanned in any weather conditions. Of course, no definition of the

83   tropopause is perfect. VHF radar system can only be limited to a few locations globally.

84   A detailed review of the close relationship between these different tropopause

85   definitions is provided by Alexander et al., (2012).

86   By means of the radiosonde, reanalysis, and satellite data available globally, long-

87   term (annual or longer) variability in tropopause height has received extensive attention

88   (e.g. Randel et al., 2000; Angell and Korshover, 2009; Son et al., 2011; Liu et al., 2014).

89   However, short period (diurnal or semidiurnal) variability of the tropopause is hard to

be examined by these measurements. In contrast, benefiting from the much higher temporal resolution, radar definition of the tropopause provides good capability for studying the diurnal and semidiurnal variation in tropopause height. Earlier, Yamamoto et al., (2003) reported the capability of the Equatorial Atmospheric Radar to examine the diurnal variation of tropopause height. Then, the diurnal variability of the tropical tropopause was investigated in detail by Das et al., (2008) using the Indian Gadanki MST radar. Its diurnal variation over a polar latitude station was investigated by Hall (2013b). In the absence of pressure and temperature parameters, the evidence of atmospheric tides can be well represented by winds (e.g. Huang et al., 2015).

The tropopause structure in midlatitudes is different from that in other regions. Double tropopauses structure is a ubiquitous feature over mid-latitude regions near 40°N (Pan et al., 2004; Randel et al., 2007). Strong evidence has revealed that the poleward intrusion of subtropical tropospheric air that occurred above the subtropical jet have resulted in the double structure (Pan et al., 2009). The higher part (second tropopause near ~16 km) is characterized by tropical features of cold and higher level, whereas the lower part (first tropopause near ~12 km) is characterized by polar features of warm and lower level. In the present study, we focus only on the first tropopauses below 16 km and these will be referred to as 'tropopause' hereafter.

In this study, using more than 5 years of Beijing MST radar echo power measurements in vertical beam, we mainly focus on the high-resolution characteristics of the tropopause structure and their comparison with the simultaneous radiosonde and dynamical definitions. Another important objective of this study is to examine the

diurnal and semidiurnal variability of the tropopause. The observational characteristics

of e.g. winds, echo power, and data acquisition rate near the tropopause layer are also

presented in the paper.

2. Data and Methods

2.1. Radar Dataset

As an important part of the Chinese Meridian Project, two MST radar systems are

designed and constructed to improve the understanding of the extratropical troposphere,

lower stratosphere, and mesosphere (Wang, 2010), which are Wuhan and Beijing MST

radars. The Beijing MST radar located in Xianghe, Hebei Province, China (39.75° N,

116.96° E, 22 m above sea level) was designed and constructed by the Institute of

Atmospheric Physics, Chinese Academy of Sciences and started its routine operation

since 20 October 2011 (Tian and Lu, 2017). The radar is a high power coherent pulse-

Doppler radar operating at 50 MHz with the maximum peak power of 172 kW and the

half-power beam width of 3.2°. Five beams are applied: one vertically pointed beam

and four 15° off-zenith beams tilted to north, east, south, and west. In order to obtain

the high-quality measurements from troposphere, lower stratosphere, and mesosphere

simultaneously, the radar is designed to operate routinely in three separate modes: low

mode (designed range 2.5-~12 km), middle mode (10-~25 km), and high mode (60-~90

km) with vertical resolutions of 150, 600, and 1200 m, respectively. Under the routine

operation, the 15-min break is followed by the 15-min operation cycle (5 min for each

mode). As a result, the time resolutions of the low, middle, and high mode

measurements are all 30 min. More detailed review of the radar system is given by

134 Chen et al. (2016).

135   Here only the low mode echo power measurements are used to determine the RT

136 height. Although the designed detectable range of the low mode is from 2.5-~12 km,

137 the vertically pointed beam can receive stronger echoes from a higher level (~14-15 km)

138 as compared with those from off-vertical beams due to the partial specular reflection

139 mechanism. The measurements in middle mode are applied to calculate the winds or

140 echo power within ~5-6 km of the tropopause. The parameters for the two routine

141 operation modes are listed in Table 1. The monthly total number of the echo power

142 profiles available in vertical beam (low mode) is shown in Fig. 1. The outliers or

143 severely contaminated data that mainly induced by system problems are eliminated.

144 The large data gap in September is due to the annual preventive maintenance.

145 **2.2. Tropopause Definitions**

146   Due to the large gradient in potential temperature, radar return power received at

147 vertical incidence is significantly enhanced upon the transition zone of the tropopause

148 layer. Using this characteristic, the RT height can be determined effectively. Here, the

149 RT is defined as the altitude (above 500 hPa) where the maximum vertical gradient of

150 echo power is located (Vaughan et al., 1995; Alexander et al., 2013; Ravindrababu et

151 al., 2014; Chen et al., 2018). Considering the occasional and random noise, to which

152 the derived-RT is sensitive, the echo power profiles are smoothed by a 3-point running

153 mean. In order to further reduce the influence of the noise, the RT definition used here

154 need to satisfy an additional criterion: the determined RT height should be continuous

155 with the adjacent RT heights (one on each side), otherwise to search for the second peak

gradient (eliminated if the second peak does not meet the additional criterion). The "continuous" here means that the discrepancy between the two successive heights (in time, 0.5-hour interval) should be <0.6 km. A typical example of the RT and LRT is illustrated in Fig. 2. The LRT is identified based on the World Meteorological Organization (WMO) criteria (WMO, 1957). The radar aspect sensitivity is expressed as the ratio between vertical (p_v) and oblique (p_o) beam (here is 15° east beam) echo power. The radiosonde soundings are launched twice daily from the Beijing Meteorological Observatory (39.93 °N, 116.28 °E, station number 54511), which is less than 45 km to the radar site. In this case, the LRT and RT consistent well and are at 11.65 km and 11.85 km respectively. As expected, the LRT characterized by a rapid increase in potential temperature gradient also corresponds to large gradient in radar aspect sensitivity. Note that the height with maximum value in echo power lie at a higher altitude than that of the RT, of ~700 m above the LRT. The dynamical tropopauses used in this paper are derived from the European Centre for Medium-Range Weather Forecasts (ECMWF) ERA-Interim Reanalysis (Dee et al., 2011) and defined as the surface of 2 PVU potential vorticity, which is same to that used by Sprenger et al., (2003) and Alexander et al. (2013).

2.3. Tropopause sharpness definition

For the compared data pairs between the RT and LRT, we calculate the corresponding tropopause sharpness that represents the strength of the tropopause inversion layer. As defined by Wirth, (2000), the tropopause sharpness S_{TP} can be calculated as:

$$S_{TP} = \frac{T_{TP+\Delta Z} - T_{TP}}{\Delta Z} - \frac{T_{TP} - T_{TP-\Delta Z}}{\Delta Z} \qquad (1)$$

where TP denotes the tropopause height, $\Delta Z = 1$ km, and T_{TP} indicates the corresponding temperature. This definition is also used in Alexander et al. 2013 and we're using it for a good comparison with our results.

3. Results

3.1. High-resolution radar tropopause structure

The height-time cross section of radar echo power and aspect sensitivity is shown in Fig. 3 for a typical month (February 2014), along with the RT, PVT and LRT marked in the figure. The RT agreed well with both the LRT and PVT in height, and most of the RT exhibit a slightly higher altitude. However, the differences between the RT and LRT are sometimes large (reach to ~1-2 km), especially when the RT experience rapid change. Regardless of the background synoptic condition, the difference in the definitions themselves is to a large degree the main contributing factor for the large difference between the RT and LRT. For example, a second layer with significant enhanced echo power is observed above the radar-derived RT for the cases on 4 and 5 February 2012 (Fig.3a). According to the definitions, the RT is well defined as the first layer with enhanced echo power and the LRT matched the second layer, similar to that observed by Yamamoto et al., (2003) and Fukao et al., (2003). It is of note that the RT well separates the troposphere characterized by low aspect sensitivity from the lower-stratosphere characterized by high aspect sensitivity (Fig.3b).

3.2. Comparisons between different definitions

To further quantify the consistency and difference in altitude between different

tropopause definitions, a detailed comparison is carried out in this section. The seasonal scatterplots for RT versus LRT and the histogram distribution of altitude differences between them are shown in Fig. 4, for the period November 2011-May 2017. A total of 2411 data pairs are obtained for comparison. Among them, the number of data pairs is 845 for DJF (winter), 721 for MAM (spring), 321 for JJA (summer), and 524 for SON (autumn). Comparisons have shown a good consistency throughout the seasons and most of the RTs exhibit a slightly higher than the LRTs. The correlation coefficient is 0.74, 0.80, 0.82, and 0.78 for DJF, MAM, JJA, and SON, respectively. The mean and standard deviation difference (RT minus LRT) calculated in DJF, MAM, JJA, and SON is (0.14±0.75), (0.26±0.78), (0.33±0.56), and (0.12±0.69) km, respectively. The proportion of the data pairs with differences <500 m is reasonably good during four seasons and is 63%, 61%, 64%, and 67% for DJF, MAM, JJA, and SON, respectively. Results of Fig. 4 indicate the potential of Beijing MST radar for detecting tropopauses throughout the seasons.

To examine the potential role of the sharpness, Fig. 5a and Fig. 5b show the histogram distribution of the tropopause sharpness along with the probability density curve for data pairs with difference (absolute values of RT minus LRT) <0.5 km and >1 km respectively. Results indicate that higher probabilities of large tropopause sharpness values occur when the RT-LRT difference is less than 0.5 km. No matter whether this distribution feature is associated with the cyclonic-anticyclonic systems (e.g. Randel et al., 2007; Randel and Wu, 2010), the results more or less demonstrate that the larger (weaker) tropopause sharpness contribute to lower (higher) difference between the RT

and LRT. From the perspective of seasonal statistics, the tropopause sharpness over Beijing station shows similar distribution characteristics throughout the seasons (not shown), which is different from that in polar regions where the sharpness is significantly higher during summer than during winter (Zängl and Hoinka, 2001).

The seasonal scatterplots and height difference histograms between the RT and PVT are illustrated and quantified in Fig. 6. The total number of comparing data pairs for winter, spring, summer, and autumn is 1422, 1260, 791, and 1145, respectively. During winter and spring (Fig. 6a and 6b), the RTs agree reasonably well with the PVTs with the correlation coefficient of 0.72 and 0.76 and the mean difference (RT minus PVT) of (0.55±0.84 km) and (1±0.89 km), respectively. In contrast, the consistency for summer and autumn (Fig. 6c and 6d) is relatively bad and with correlation coefficient of 0.33 and 0.47 and mean difference of (0.80±1.39 km) and (0.75±1.23 km), respectively. Especially for summer, the proportion of the comparing data pairs with difference <0.5 km is only 10.6% (84).

3.3. Observational characteristics in the vicinity of tropopause

Middle mode radar measurements are used for examining the horizontal wind, return power, and effective wind data acquisition rate within 5-6 km of the tropopause (upper troposphere and lower stratosphere). Left panels of Fig. 7 show the vertical scatterplots of the static stability (represented by the buoyancy frequency squared) as a function of height relative to the LRT and right panels show the radar echo power as a function of height relative to the RT, during two specific years 2012-2013 for extended winter NDJFM and summer MJJAS seasons. Mean and standard deviations are also

244   plotted in each panel of Fig. 7. Results clearly show sudden jump in static stability and

245   radar power near the tropopause layer. The sudden increase in echo power is more

246   gradual than that in static stability. The amplitude of the sudden increase in radar power

247   experienced a slightly larger during NDJFM than that during MJJAS (red lines of right

248   panels). Another interesting feature in the lower-stratosphere is that the static stability

249   show less disperse during NDJFM than that during MJJAS.

250   Fig. 8 shows the profiles of mean data acquisition rate in radar wind for low and

251   middle modes during November 2011-May 2017. Both profiles exhibit a sudden

252   increase with height near the tropopause, with the first peak located ~1 km higher above

253   the mean tropopause height. Note that the second inversion in middle mode profile that

254   occurred near 16 km is associated with the second tropopause. As limited by the highest

255   detectable altitude (the data acquisition rate decreased to lower than 20% at ~16 km),

256   the profile in low mode shows little evidence of second inversion.

257   Fig. 9 shows time-height intensity plot of the monthly mean radar-derived

258   horizontal wind during November 2011-May 2017, together with the monthly mean

259   location of RT and LRT. The monthly mean RT and LRT agreed well with each other

260   in height, within 400 m in August and September and even lower in other months of

261   about within 200 m. They both exhibit a clear seasonal variation, with maximum in

262   early autumn of ~11.6 km and minimum in early spring of ~10.3 km. The monthly mean

263   wind jet varies with season, with the thinnest thickness and lowest strength in summer.

264   The mean tropopause height corresponds to the lower boundary location of peak wind

265   layer. The error bars of both the RT and LRT help to illustrate that the tropopauses

266   changes by larger amplitude in winter and June than that in other months.

267   **3.4.   Periodogram analysis of the radar tropopause**

268   High temporal resolution detection of tropopause by VHF radar have allowed us

269   to investigate the diurnal or semidiurnal variability of the tropopause. Atmospheric tides

270   are well known global oscillations contributing to the diurnal variation in temperature

271   and background winds, which in turn modulate the tropopause height. With the absence

272   of temperature measurements, zonal and meridional winds are applied to demonstrate

273   the evidence of diurnal or semidiurnal modulation by tidal. The frequency power

274   spectrum of the RT height, zonal and meridional wind, calculated by means of Lomb-

275   Scargle method (Press and Rybicki, 1989), is illustrated in Fig. 10 for two typical

276   months: May 2015 and December 2016. Lomb-Scargle algorithm is applied due to the

277   presence of data gaps (~2 days per week, especially during 2012-2013). The dominant

278   ~24 h periodicity in all the three parameters is obvious for both months. The evidence

279   of ~12 h period is observed for May 2015 (Fig. 10a), although the power is relatively

280   weaker. Through the analysis for each individual month, we found that the semidiurnal

281   component in the three parameters is generally and occasionally observed in summer

282   and later spring during our experimental period. Characteristics of the diurnal variation

283   in RT height can be better represented in Fig. 11, which shows the mean Lomb-Scargle

284   power spectrum of the RT as a function of month during November 2011-May 2017.

285   As compared with other months, the dominant diurnal periodicity is less evident in

286   April. We need to clarify that atmospheric tides are of course not the only source of the

287   diurnal variation in tropopause height, diurnal convective activities (Yamamoto et al.,

288 2003) might also be an important cause. Here will not be discussed in detail.

289

290 **4. Discussion**

291   As for the radar echo power definition, the RT estimation sometimes will fail due

292 to the system problems, even if the thermal tropopause is well defined (Hall et al., 2009).

293 Apart from the system problems (e.g. the damage of T/R module), the following two

294 conditions are primarily responsible for the failure (or difficulty) of both the radar and

295 thermal definitions over the radar site latitude (~40° N). Firstly, the temperature

296 sometimes continued to decrease until to the stratosphere (above 16 km) in summer and

297 early autumn, leading to the failure/difficulty of both the radar and thermal definitions

298 (a typical case as shown in Fig. 12a). Need to note that the temperature inversion layer

299 occurred at ~16 km in summer or early autumn is the second tropopause with

300 characteristics of Tropics (Pan et al., 2004; Randel et al., 2007). Secondly, some specific

301 meteorological processes can lead to the ambiguities and indefiniteness in thermal and

302 radar definitions, such as fronts, cyclones or typhoons, and folding (e.g. Nastrom et al.,

303 1989; May et al., 1991; Roettger, 2001; Alexander et al., 2013). Such ambiguities often

304 result in large difference in altitude between the RT and LRT. Apart from the situations

305 above, another condition is also commonly responsible for the difficult in identifying

306 the thermal tropopause from radiosonde profiles during summer. As a typical case

307 shown in Fig. 12b, a significant inversion in temperature (at ~12 km) is recorded from

308 the radiosonde profile, but the altitude extent of inversion layer is too thin to meet the

309 WMO criterion that thermal definition required. Whereas, the apparent enhancement in

radar echo power corresponding to such inversion layer is strong enough to well define

the RT. The temperature inversion located near ~16 km (the second tropopause) is not

the focus of this paper.

Pan et al., (2004) have reported that the difference between the LRT and PVT are

more distinct in the vicinity of subtropical jet. In the northern hemisphere, the axis of

the subtropical jet is situated near ~30°N in spring and winter, whereas in summer and

early autumn the subtropical jet shifts northward to ~40°N (see Fig. 4 in Ding and Wang,

2006). We preliminary considered that the inconsistency between the RT and PVT in

summer and early autumn (Fig. 6c and 6d) is most likely related to the subtropical jet

shifting poleward to ~40°N. The existing cyclones or anticyclones in the upper-

troposphere (Wirth, 2000), of course, may also be an important influence factor for the

significant asymmetric differences (most of the scattered points deviate significantly

from the 1:1 line). The asymmetric differences, that is most of the RT are located higher

than the 2PVU tropopause height, suggest that the 2PVU surface is not the best measure

of a dynamical tropopause over Beijing during summer-time. More detailed discussion

about the striking asymmetric differences in height between LRT and PVT can be seen

in Wirth (2001) and will not be given here. Anyway, we need to be careful when using

the 2PVU dynamical definition to define the tropopause over radar site latitude ~40° N,

especially in summer.

About the characteristics of tropopause and the comparison between different

definitions, there are many differences between mid-latitude and polar regions. In mid-

latitude (~40°N), our results show that: (1) the agreement between RT and LRT is

similar good throughout the seasons; (2) RTs are generally located higher than the LRT;
(3) the thermal definition sometimes fail in summer and early autumn; (4) the
agreement between the RT/LRT and PVT in summer is poor. Whereas, in contrast,
previous researches about the tropopause over polar regions reported that (Wirth, 2000;
Alexander et al., 2013): (1) the difference between the RT and LRT is larger during
winter than that during summer; (2) RTs are generally located lower than the LRT; (3)
the thermal definition sometimes fail in winter and spring; (4) the comparison between
the RT and PVT showed the similar good agreement during both summer and winter.

Over a polar latitude station, the seasonal characteristics of the diurnal oscillation
in tropopause height were investigated using 5 years of SOUSY VHF radar
measurements (Hall, 2013b). The sunlight variability in polar regions is different from
that in other latitudes of the world. Different sunlight variation actually will lead to
difference in atmospheric tides, and then would result in different diurnal variation in
tropopause height. Here we found that the diurnal oscillation of RT height at Xianghe
is ubiquitous and obvious throughout the seasons except for April (Fig. 11). Whereas at
polar latitude and in months of November to February when there is no sunlight, Hall
(2013b) observed little evidence of 24 h diurnal variability in RT height.

5. Conclusions

In this paper, we present the high resolution structure and variability of the
tropopause in Xianghe, China (39.75° N, 116.96° E), based on the Beijing MST radar
vertical beam echo power data collected during the period November 2011-May 2017.

354 Fine-scale structure of the RT is well determined with a high temporal resolution of 0.5

355 h. Comparison results have shown good agreement in altitude between the RT and LRT,

356 with a correlation coefficient of ≥ 0.74 for the four seasons. Higher tropopause

357 sharpness seems to contribute lower difference between the RT and LRT in altitude and

358 weaker sharpness appears responsible for higher difference. The agreement between

359 the RT and PVT is relatively well in winter and spring with correlation coefficient of

360 0.72 and 0.76 respectively, but poor during summer with a correlation coefficient of

361 only 0.33. We initially suggested that the poor consistency between RT and PVT is

362 associated with the subtropical jet shifting poleward to ~40°N.

363 As expected, the sudden jump in static stability (represented by the buoyancy

364 frequency squared) and the rapid increase in radar echo power upon the tropopause

365 layer are clearly observed. Upon the tropopause layer, a sudden increase in effective

366 radar data acquisition rate is also observed. Both the monthly mean RT and LRT height

367 have shown a clear seasonal variation. The variability and oscillation of RT height with

368 diurnal or lower timescales is presented. Obvious diurnal variation in tropopause height,

369 zonal wind, and meridional wind is generally observed throughout the seasons,

370 indicating the modulation most likely from the atmospheric tides. The semidiurnal

371 variation in RT height is not so obvious and commonly observed occasionally in

372 summer and late spring.

373

374 **Data availability.**

375 MST radar data are publicly and freely available at http://159.226.22.74/ (MST, 2019).

376 ECMWF ERA-interim data are publicly and freely available at

377 https://www.ecmwf.int/en/forecasts/datasets (ECMWF, 2019). Global radiosonde data

378 are publicly available from the NOAA/ESRL Database at https://ruc.noaa.gov/raobs/

379 (Radiosonde, 2019).

380 **Author contributions.**

381 FC originally conceived and designed the study, in consultation with GC. The

382 processing and data analysis for radar, radiosonde, and reanalysis data was developed

383 by FC. GC, YT, SZ, and KH are the people in charge of MST radar data archiving,

384 mage-generation and quality control. CW and WZ helped to check the manuscript.

385 **Acknowledgment**.

386 This work is funded by National Natural Science Foundation of China (NSFC grants

387 No. 41474132 and 41722404). We acknowledge the Chinese Meridian Project for

388 providing the MST radar data. The authors sincerely acknowledge the ECMWF for

389 providing global reanalysis data.

390

391 **References**

392 Alexander, S.P., Murphy, D.J., and Klekociuk, A.R.: High resolution VHF radar

393   measurements of tropopause structure and variability at Davis, Antarctica (69° S,

394   78° E), Atmos. Chem. Phys., 13, 3121-3132, 2013.

395   Angell, J. K., and Korshover, J.: Quasi-biennial and long-term fluctuations in

396   tropopause pressure and temperature, and the relation to stratospheric water vapor

397   content. Monthly Weather Review, 102(1), 29-34, 2009.

398   Appenzeller, C., Holton, J. R., and Rosenlof, K. H.: Seasonal Variation of Mass

399   Transport Across the Tropopause. Journal of Geophysical Research, 101(D10),

400   15071-15078, 1996.

401   Añel, J. A., J. C. Antuña, L. de la Torre, R. Nieto, and Gimeno L.: Changes in

402   tropopause height for the Eurasian region determined from CARDS radiosonde

403   data. Naturwissenschafte, 93, 603–609, doi:10.1007/s00114-006-0147-5, 2006.

404   Bethan, S., Vaughan, G., and Reid, S. J.: A comparison of ozone and thermal tropopause

405   heights and the impact of tropopause definition on quantifying the ozone content

406   of the troposphere. Quarterly Journal of the Royal Meteorological Society,

407   122(532), 929-944, 1996.

408   Baray, J., Daniel, V., Ancellet, G., and Legras, B.: Planetary-scale tropopause folds in

409   the southern subtropics. Geophysical Research Letters, 27(3), 353-356, 2000.

410   Chen, F. L., Chen, G., Shi, C. H., Tian, Y. F., Zhang, S. D., and Huang, K. M.: Strong

411   downdrafts preceding rapid tropopause ascent and their potential to identify cross-

412   tropopause stratospheric intrusions, Annales Geophysicae, 36(5), 1403-1417,

413   2018.

414   Chen, G., Cui, X., Chen, F., Zhao, Z., Wang, Y., Yao, Q., and Gong, W.: MST Radars

415   of Chinese Meridian Project: System Description and Atmospheric Wind

416   Measurement. IEEE Transactions on Geoscience and Remote Sensing, 54(8),

417   4513-4523, 2016.

418   Das, S. S., Jain, A. R., Kumar, K. K., and Rao, D. N.: Diurnal variability of the tropical

419   tropopause: Significance of VHF radar measurements. Radio Science, 43(6), 1-14,

420   doi:10.1029/2008RS003824, 2008.

421   Dee, D. P., Uppala, S. M., Simmons, A. J., Berrisford, P., Poli, P., Kobayashi, S. et al.:

422   The ERA-Interim reanalysis: configuration and performance of the data

423   assimilation system. Quarterly Journal of the Royal Meteorological Society,

424   137(656), 553-597, 2011.

425   Ding, A., and Wang, T.: Influence of stratosphere-to-troposphere exchange on the

426   seasonal cycle of surface ozone at Mount Waliguan in western China. Geophysical

427   Research Letters, 33(3), 233-252, doi:10.1029/ 2005GL024760, 2006.

428   Fukao, S., H. Hashiguchi, M. Yamamoto, T. Tsuda, T. Nakamura, M. K. Yamamoto,

429   T. Sato, M. Hagio, and Y. Yabugaki:. Equatorial Atmosphere Radar (EAR):

430   System description and first results. Radio Science, 38(3), 1053, 2003.

431   Gage, K. S., and Green, J. L.: An objective method for the determination of tropopause

432   height from VHF radar observations. Journal of Applied Meteorology, 21(21),

433   1150-1154, 1982.

434   Gage, K. S., and Green, J. L.: Tropopause Detection by Partial Specular Reflection with

435   Very-High-Frequency Radar. Science, 203(4386), 1238-1240, 1979.

436   Gettelman, A., P. Hoor, L. L. Pan, W. J. Randel, M. I. Hegglin, and T. Birner: The

437   extratropical upper troposphere and lower stratosphere, Reviews of Geophysics,

438   49(3), RG3003, doi: 10.1029/2011RG000355, 2011.

Hermawan, E., Tsuda, T., and Adachi, T.: MU radar observations of tropopause variations by using clear air echo characteristics. Earth, Planets and Space, 50(4), 361-370, 1998.

Hall, C.: The radar tropopause above Svalbard 2008–2012: Characteristics at various timescales. Journal of Geophysical Research, 118(6), 2600-2608, 2013a.

Hall, C.: The radar tropopause at 78°N, 16°E: Characteristics of diurnal variation. Journal of Geophysical Research, 118(12), 6354-6359, doi:10.1002/jgrd.50560, 2013b.

Hall, C. M., Röttger, J., Kuyeng, K., Sigernes, F., Claes, S., and Chau, J. L.: Tropopause altitude detection at 78°N, 16°E, 2008: First results of the refurbished SOUSY radar. Radio Science, 44(5), 1-12, doi:10.1029/ 2009RS004144, 2009.

Hoinka, K. P.: Statistics of the Global Tropopause Pressure. Monthly Weather Review, 126(12), 3303-3325, 1998.

Hoskins, B. J., Mcintyre, M. E., and Robertson, A. W.: On the use and significance of isentropic potential vorticity maps. Quarterly Journal of the Royal Meteorological Society, 111(470), 877-946, 2007.

Huang, C., Zhang, S. D., Zhou, Q. H., Yi, F., Huang, K., Gong, Y., Zhang, Y., and Gan, Q.: WHU VHF radar observations of the diurnal tide and its variability in the lower atmosphere over Chongyang (114.14° E, 29.53° N), China. Annales Geophysicae, 33(7), 865-874, 2015.

Hoerling, M. P., Schaack, T. K., and Lenzen, A. J.: Global Objective Tropopause Analysis. Monthly Weather Review, 119(8), 1816-1831, 1991.

461 Liu, Y., Xu, T., and Liu, J.: Characteristics of the seasonal variation of the global

462   tropopause revealed by cosmic/GPS data. Advances in Space Research, 54(11),

463   2274-2285, 2014.

464 May, P. T., Yamamoto, M., Fukao, S., Sato, T., Kato, S., and Tsuda, T.: Wind and

465   reflectivity fields around fronts observed with a VHF radar. Radio Science, 26(5),

466   1245-1249, 1991.

467 Nastrom, G. D., Green, J. L., Gage, K. S., and Peterson, M. R.: Tropopause Folding

468   and the Variability of the Tropopause Height as Seen by the Flatland VHF Radar.

469   Journal of Applied Meteorology, 28(12), 1271-1281, 1989.

470 Nielsen-Gammon, J. W.: A visualization of the global dynamic tropopause. Bulletin of

471   the American Meteorological Society, 82(6), 1151-1168, 2001.

472 Pan, L. L., Randel, W. J., Gary, B. L., Mahoney, M. J., and Hintsa, E. J.: Definitions

473   and sharpness of the extratropical tropopause: A trace gas perspective. Journal of

474   Geophysical Research, 109, D23103, doi:10.1029/2004JD004982, 2004.

475 Pan, L. L., W. J. Randel, J. C. Gille, W. D. Hall, B. Nardi, S. Massie, V. Yudin, R.

476   Khosravi, P. Konopka, and D. Tarasick: Tropospheric intrusions associated with

477   the secondary tropopause, Journal of Geophysical Research, 114, D10302, 2009.

478 Press, W. H., and Rybicki, G. B.: Fast algorithm for spectral analysis of unevenly

479   sampled data. The Astrophysical Journal, 338(1), 277-280, 1989.

480 Ravindrababu, S., Venkat Ratnam, M., Sunilkumar, S. V., Parameswaran, K., and

481   Krishna Murthy, B. V.: Detection of tropopause altitude using Indian MST radar

482   data and comparison with simultaneous radiosonde observations. Journal of

483   Atmospheric and Solar-Terrestrial Physics, 121(6), 679-687, 2014.

484 Randel, W. J., Wu, F., and Gaffen, D. J.: Interannual variability of the tropical

485   tropopause derived from radiosonde data and NCEP reanalyses. Journal of

486   Geophysical Research Atmospheres, 105(D12), 15509-15523, 2000.

487 Randel, W. J., Seidel, D. J., and Pan, L. L.: Observational characteristics of double

488   tropopauses. Journal of Geophysical Research, 112, D07309, 2007.

489 Randel, W. J., and Wu, F.: The Polar Summer Tropopause Inversion Layer. Journal of

490   the Atmospheric Sciences, 67(8), 2572-2581, 2010.

491 Randel, W. J., Wu, F., and Forster, P. M.: The extratropical tropopause inversion layer:

492   Global observations with GPS data, and a radiative forcing mechanism. Journal of

493   the Atmospheric Sciences, 64(12), 4489-4496, 2007.

494 Ramakrishnan, K. P.: Distortion of the tropopause due to meridional movements in the

495   sub-stratosphere. Nature, 132(3346), 932-932, 1933.

496 Roettger, J.: Observations of the polar d-region and the mesosphere with the Eiscat

497   Svalbard radar and the SOUSY Svalbard Radar (scientific paper). Memoirs of

498   National Institute of Polar Research. Special Issue, 54(94), 9-20, 2001.

499 Reed, R. J.: A study of a characteristic tpye of upper-level frontogenesis. Journal of the

500   Atmospheric Sciences, 12(3), 226-237, 1955.

501 Santer, B. D., Wehner, M. F., Wigley, T. M., Sausen, R., Meehl, G. A., Taylor, K. E.,

502   Ammann, C., Arblaster, J., Washington, W. M., Boyle, J. S., and Brüggemann, W.:

503   Contributions of anthropogenic and natural forcing to recent tropopause height

504   changes. Science, 301(5632), 479-483, 2003.

505   Santer, B. D., Sausen, R., Wigley, T. M., Boyle, J. S., Achutarao, K., Doutriaux, C.,

506   Hansen, J. E., Meehl, G. A., Roeckner, E., Ruedy, R., Schmidt, G., and Taylor, K.

507   E.: Behavior of tropopause height and atmospheric temperature in models,

508   reanalyses, and observations: Decadal changes. Journal of Geophysical Research,

509   108(D1), 4002, doi:10.1029/2002JD002258, 2003a.

510   Sausen, R., and Santer, B. D.: Use of Changes in Tropopause Height to Detect Human

511   Influences on Climate. Meteorologische Zeitschrift, 12(3), 131-136, 2003.

512   Schmidt, T., Heise, S., Wickert, J., Beyerle, G., & Reigber, C.: GPS radio occultation

513   with CHAMP and SAC-C: global monitoring of thermal tropopause parameters.

514   Atmospheric Chemistry and Physics, 5(6), 1473-1488, 2005.

515   Seidel, D. J., Ross, R. J., Angell, J. K., and Reid, G. C.: Climatological characteristics

516   of the tropical tropopause as revealed by radiosondes. Journal of Geophysical

517   Research, 106(D8), 7857-7878, 2001.

518   Son, S. W., Tandon, N. F., & Polvani, L. M.: The fine-scale structure of the global

519   tropopause derived from COSMIC GPS radio occultation measurements. Journal

520   of Geophysical Research: Atmospheres, 116(D20), 2011.

521   Sprenger, M., Croci Maspoli, M., and Wernli, H.: Tropopause folds and cross-

522   tropopause exchange: a global investigation based upon ECMWF analyses for the

523   time period March 2000 to February 2001. Journal of Geophysical Research

524   Atmospheres, 108(12), 291-302, 2003.

525   Tian, Y., and Lu, D.: Comparison of Beijing MST Radar and Radiosonde Horizontal

526   Wind Measurements. Advances in Atmospheric Sciences, 34(1), 39-53. doi:

527   10.1007 / s00376-016-6129-4, 2017.

528 Vaughan, G., Howells, A., and Price, J. D.: Use of MST radars to probe the mesoscale

529   structure of the tropopause. Tellus A, 47(5), 759-765, 1995.

530 Wang, C.: Development of the Chinese meridian project. Chinese Journal of Space

531   Science, 30(4), 382–384, 2010.

532 Wilcox L.J., Hoskins B.J., Shine K.P. 2012. A global blended tropopause based on ERA

533   data. Part I: Climatology. Q. J. R. Meteorol. Soc. 138: 561–575.

534   DOI:10.1002/qj.951.

535 Wirth, V.: Thermal versus dynamical tropopause in upper-tropospheric balanced flow

536   anomalies. Quarterly Journal of the Royal Meteorological Society, 126(562), 299-

537   317, 2000.

538 Wirth, V.: Cyclone-anticyclone asymmetry concerning the height of the thermal and the

539   dynamical tropopause. Journal of the Atmospheric Sciences, 58(1), 26-37, 2001.

540 WMO: Definition of the tropopause. WMO Bull., 6, 136, 1957.

541 Yamamoto, M., Oyamatsu, M., Horinouchi, T., Hashiguchi, H., and Fukao, S.: High

542   time resolution determination of the tropical tropopause by the Equatorial

543   Atmosphere Radar. Geophysical Research Letters, 30(21), 2094, 2003.

544 Zängl, G., and Hoinka, K. P.: The tropopause in the polar regions. Journal of Climate,

545   14(2001), 3117-3139, 2001.

546

547 **Table**

Radar parameter	Value
Transmitted frequency	50 MHz
Antenna array	24×24 3-element Yagi
Antenna gain	33 dB
Transmitter peak power	172 kW
Code	16-bit complementary
No. coherent integrations	128 (low mode)/64 (mid mode)
No. FFT points	256
No. spectral average	10
Pulse repetition period	160 (low mode)/320 (mid mode) μs
Half power beam width	3.2^o
Pulse length	1 (low mode)/4 (mid mode) μs
Range resolution	150 (low mode)/600 (mid mode) m
Temporal resolution	30 min
Off-zenith angle	15°

548 **Table 1.** Routine operational parameters in low and middle mode for the Beijing MST

549 radar used in this study.

550

551 **Figures**

552
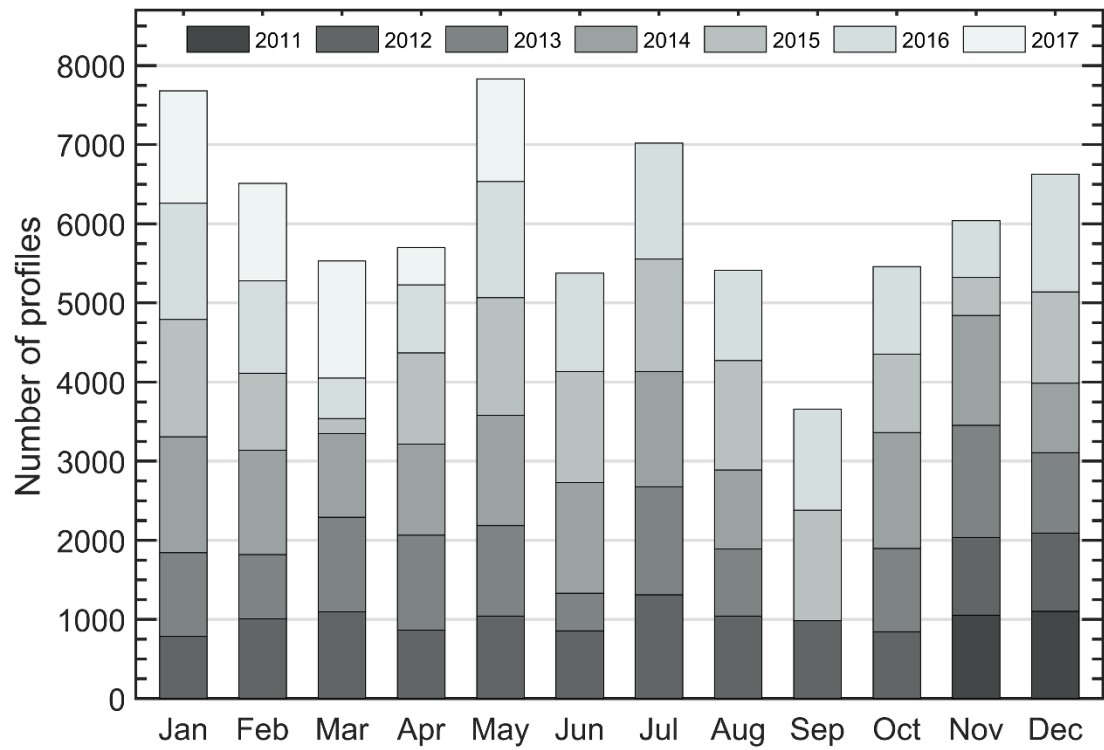
553 **Figure 1.** Distribution of the monthly total number of radar return echo power profiles

554 that available from vertical beam in low mode, collected for the period November 2011-
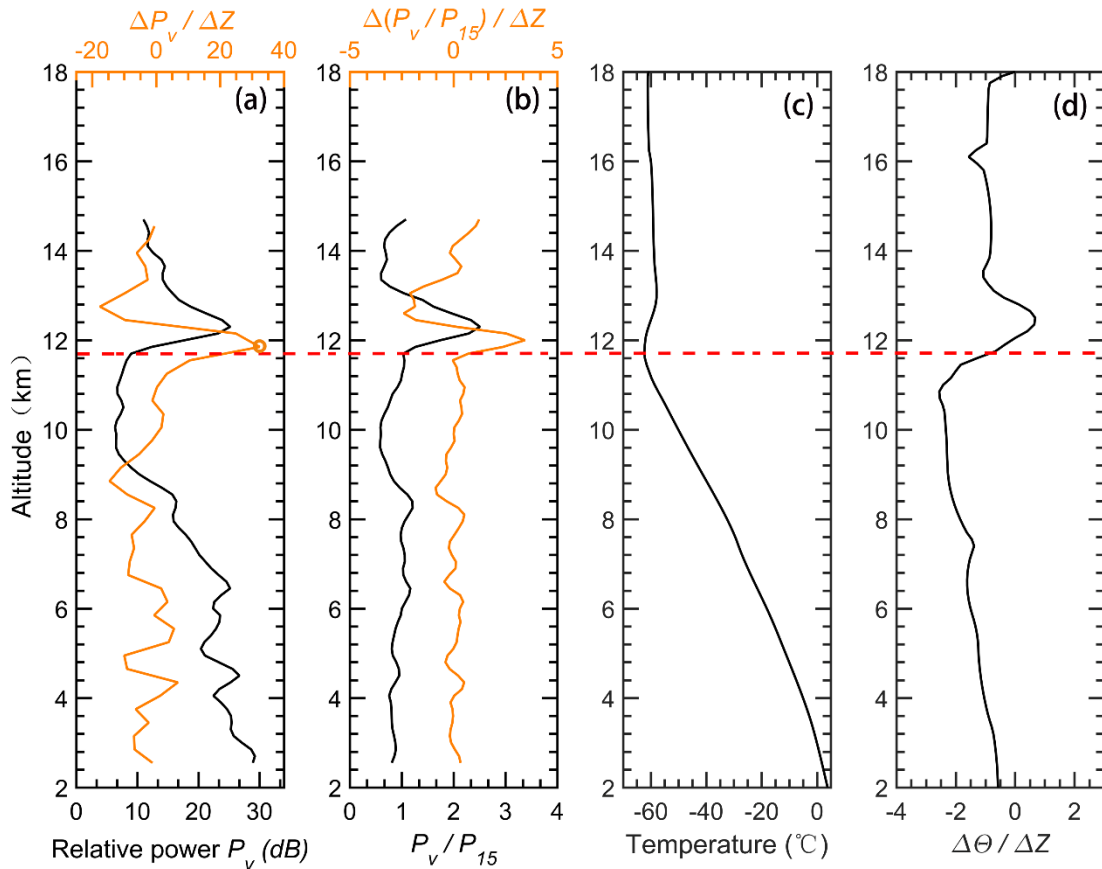
555 May 2017.

Figure 2. Example vertical profiles of (a) relative radar echo power (black line) along with its gradient variation (orange line), (b) radar aspect sensitivity (black line) along with its gradient variation (orange line), (c) radiosonde temperature and (d) potential temperature gradient on 00 UT 04 November 2011. The horizontal red dashed line marks the LRT height. The orange circle in (a) denotes the RT height.

564
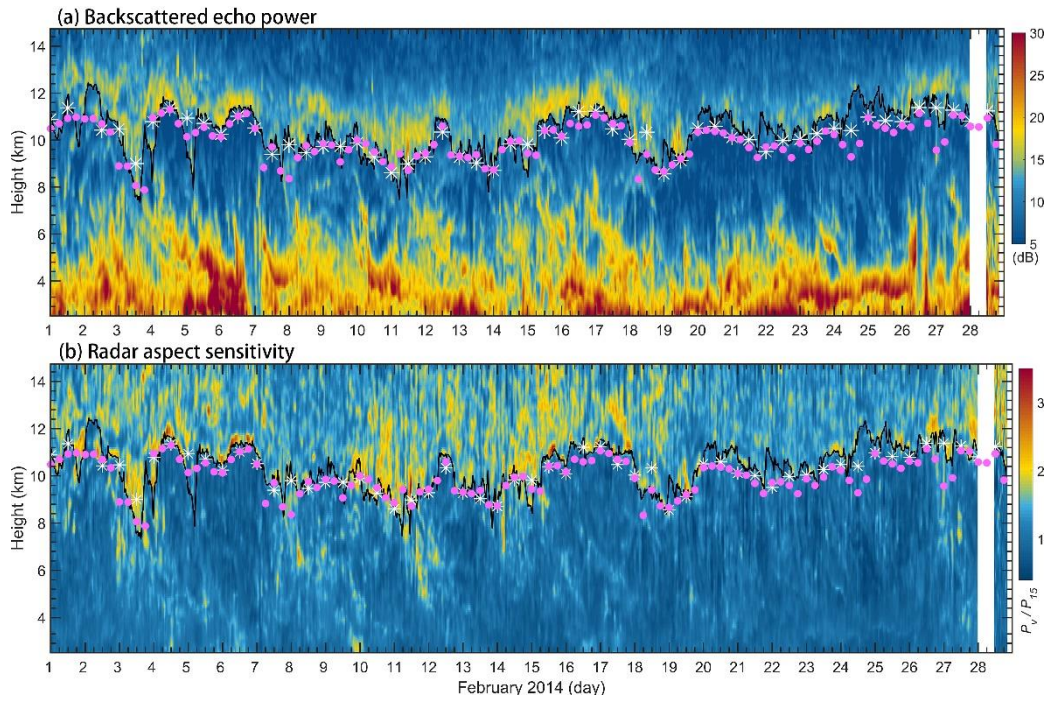
Figure 3. Altitude-time intensity plot of (a) radar backscattered echo power and (b)

radar aspect sensitivity for February 2014. The tropopauses determined based on the

radar echo definition are shown as a black solid curve. The white asterisks '*' and pink

dots indicate the location of the LRT derived from simultaneous twice daily radiosonde

data and the PVT from ECMWF ERA-Interim reanalysis, respectively. White stripe

indicates the time frame of radar missing data.

571

572
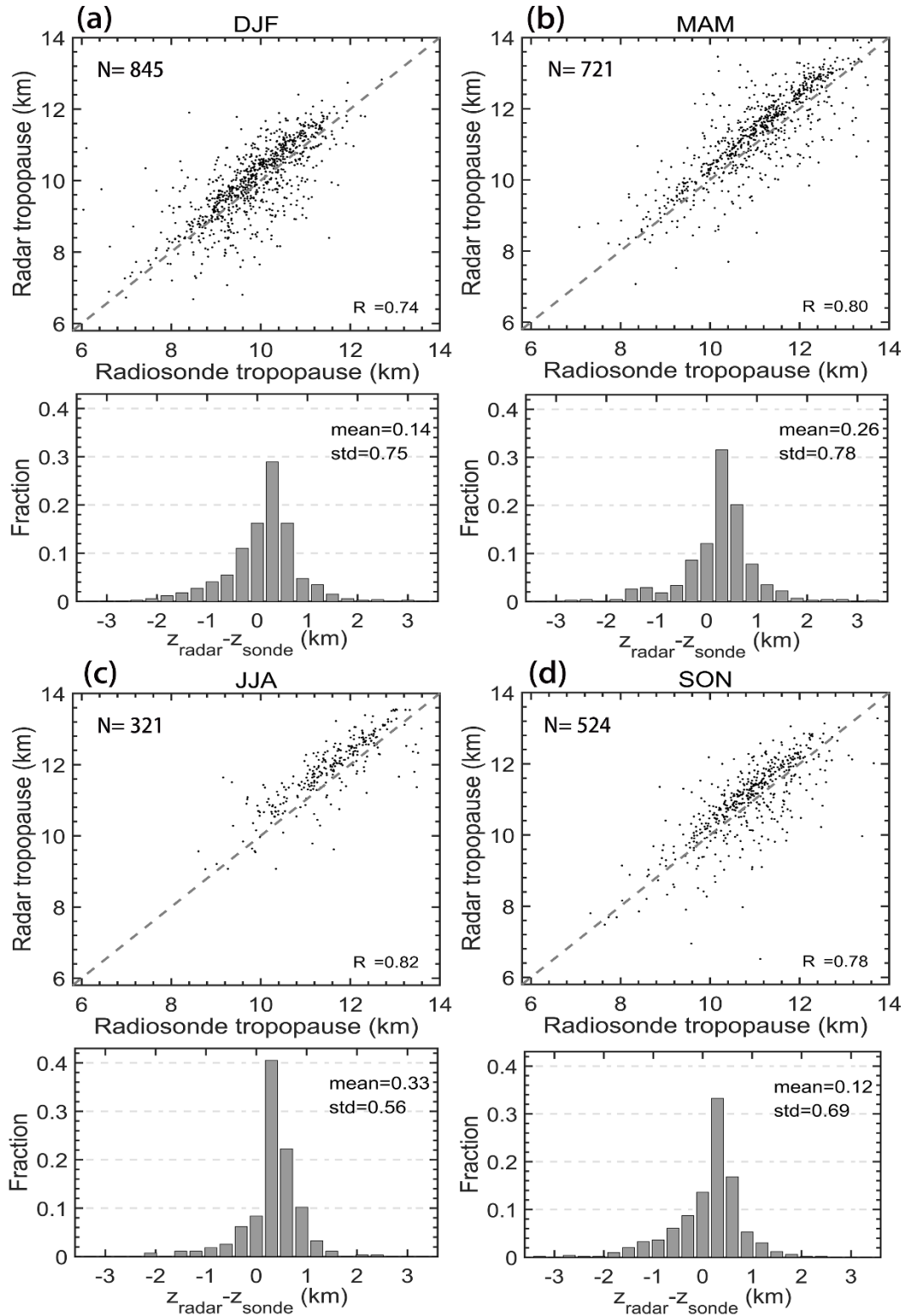
Figure 4. Seasonal scatterplots of the RT versus LRT and histogram distribution of

altitude differences between the RT and the LRT, for (a) winter DJF, (b) spring MAM,

(c) summer JJA, and (d) autumn SON, during the period November 2011-May 2017.

576   The positive values in the histogram indicate the RT locating at a higher level than the

577   LRT. The grey dashed line shows the 1:1 line. Here, 'N','R^2', 'mean', and 'std' indicate

578   the sample numbers, correlation coefficient, mean difference, and standard deviation of

579   the difference, respectively.
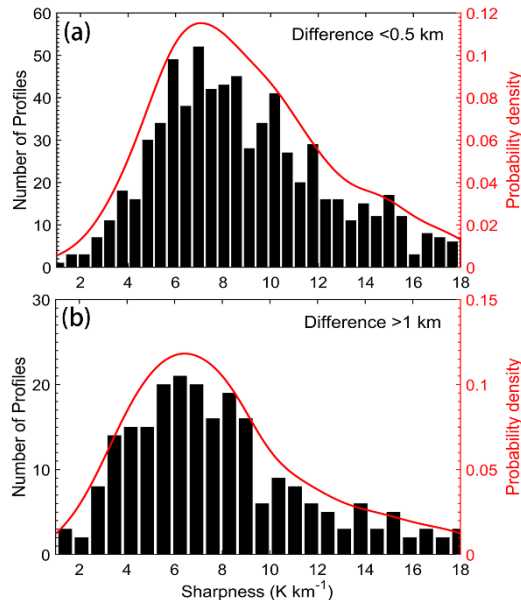
580

581   **Figure 5.** Histogram distribution of the tropopause sharpness for (a) difference <0.5

582   km, and (b) >1 km respectively between the LRT and the RT.

583

584
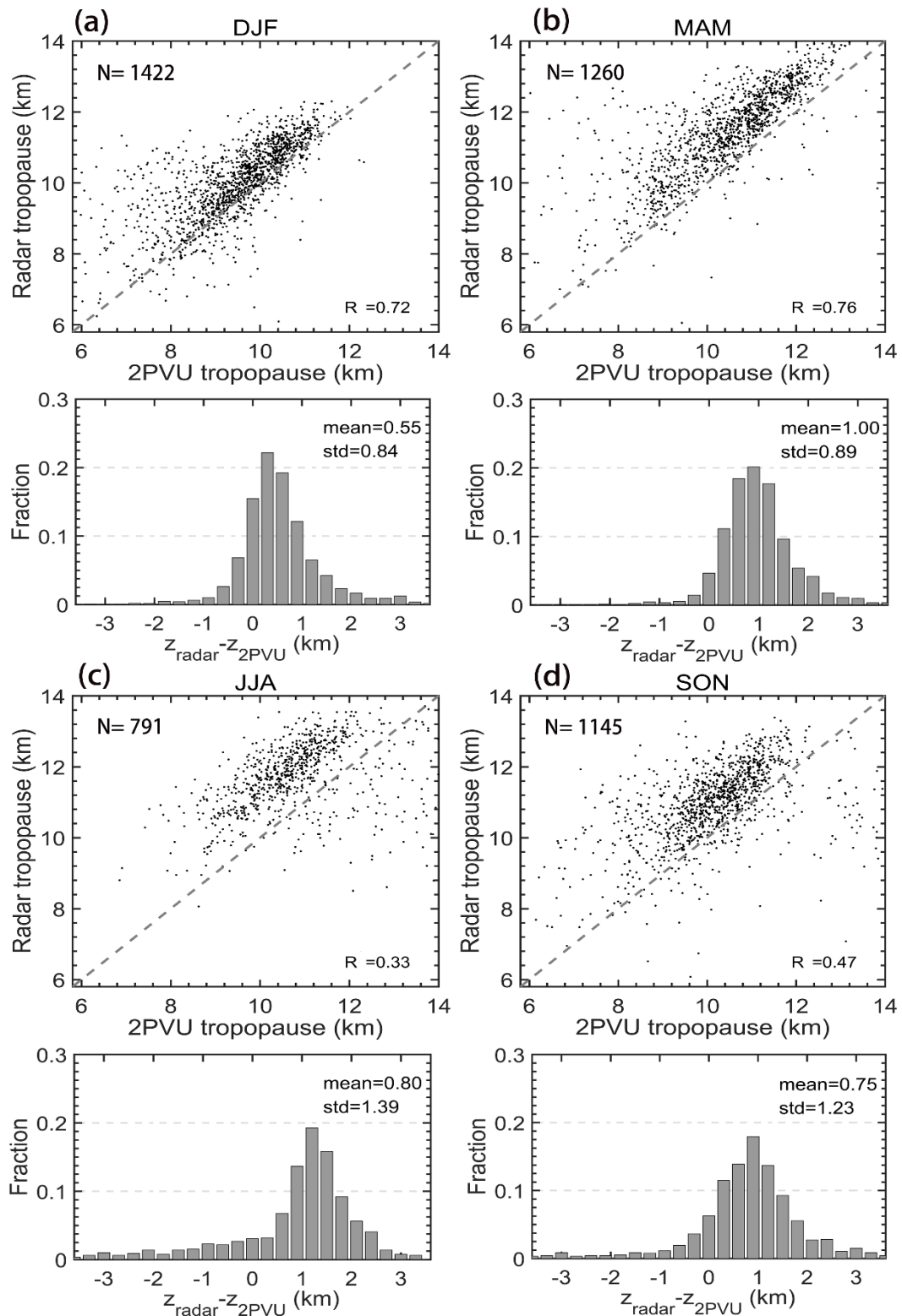
Figure 6. Same as figure 4, but for the comparison between the RT and the PVT.

586

587
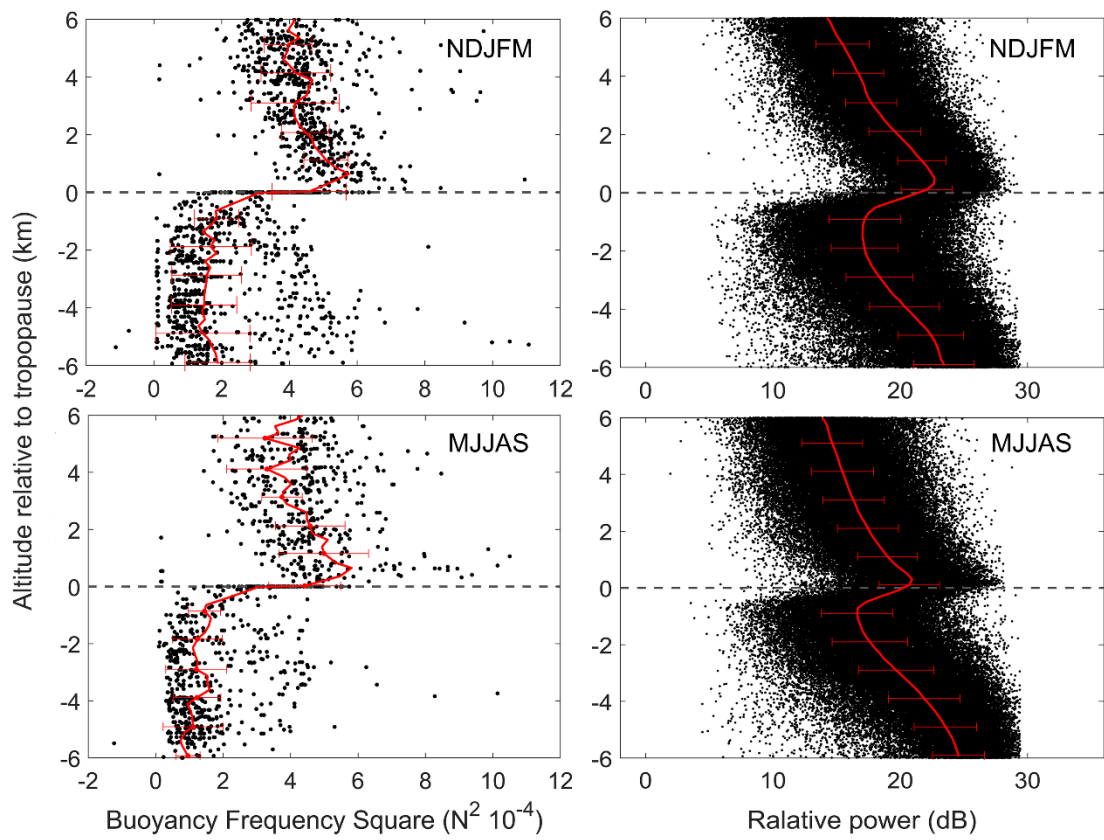
Figure 7. Scatterplots of (left panels) static stability (N^2) and (right panels) radar

relative echo power as a function of altitude relative to the LRT (left panels) and RT

(right panels) for extended winter (NDJFM) and summer (MJJAS) seasons for two

specific years 2012-2013. Red lines in each panel denote the corresponding mean

profiles and the error bars indicate the standard deviations.

593

594

595
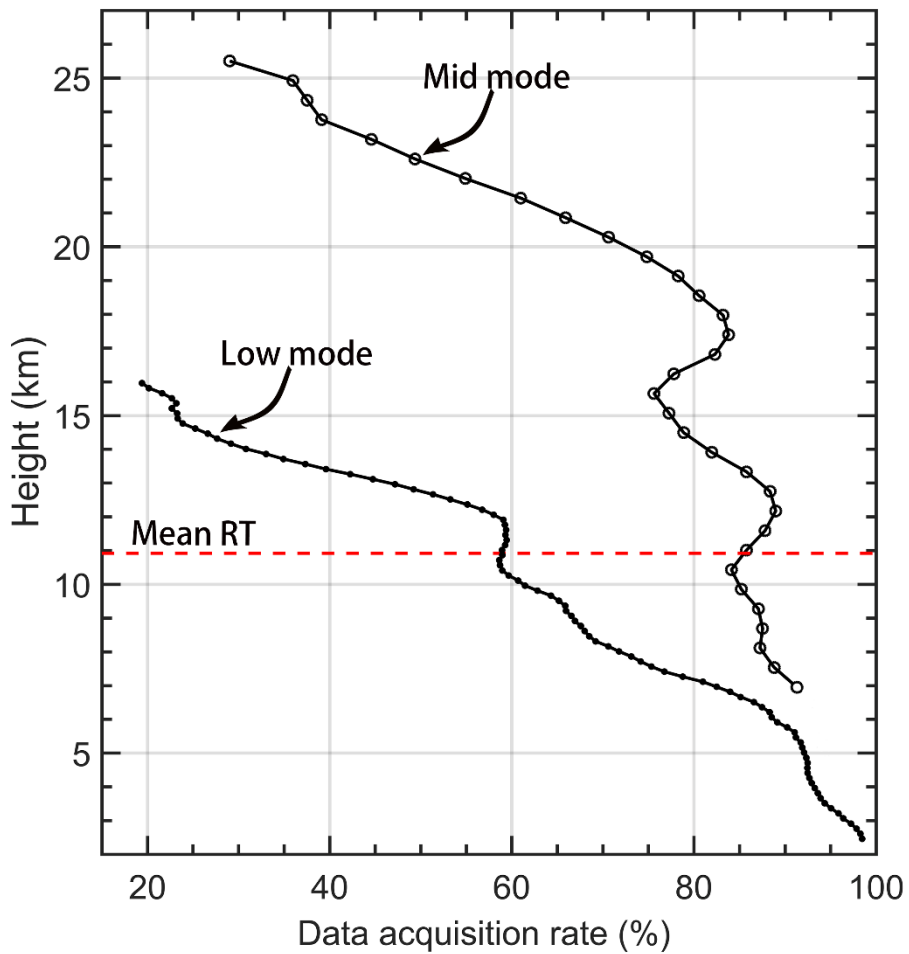
Figure 8. Vertical height profiles of the averaged effective radar wind data acquisition

rate in low mode and middle mode during November 2011-May 2017. The red dashed

line indicates the mean RT height.

599
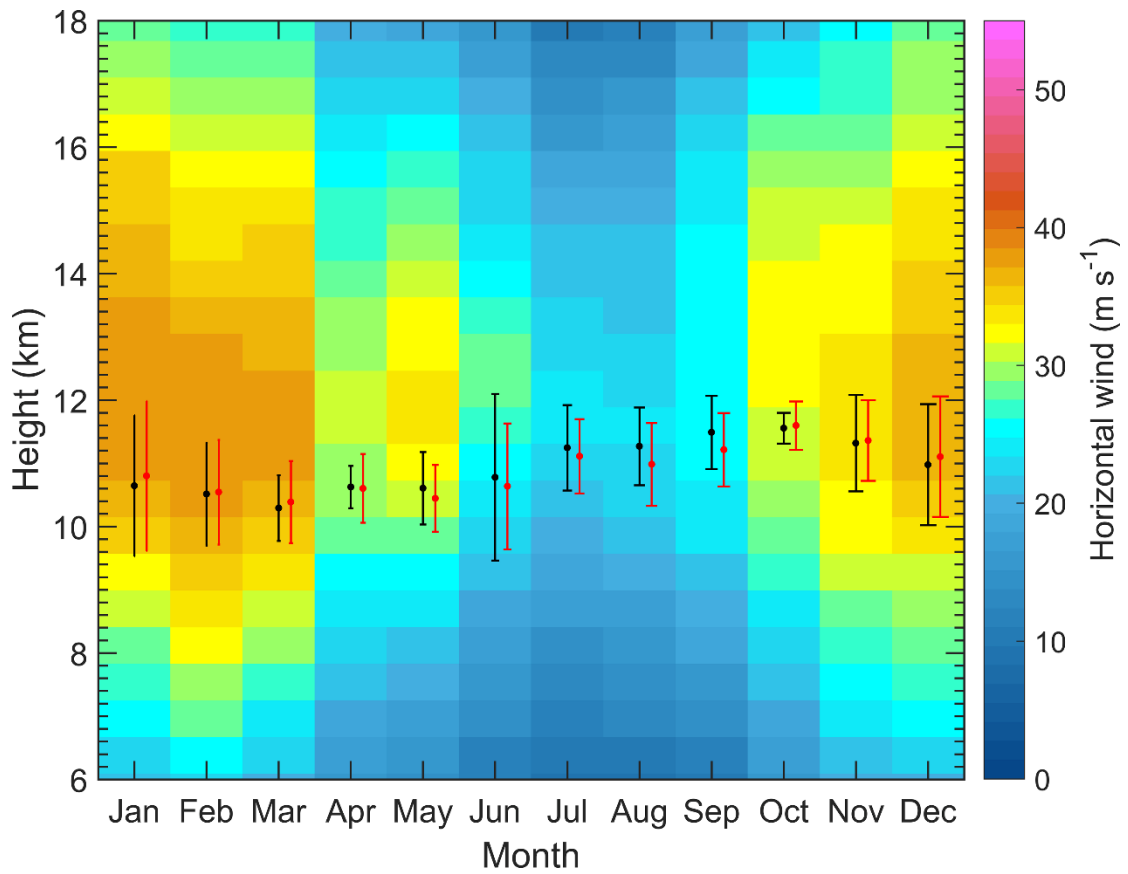
Figure 9. Height-time intensity map of monthly mean horizontal wind speed (shaded,

m/s) derived from the middle mode of Beijing MST radar, during November 2011-May

2017. Also shown is the monthly mean height of RT (black dots) and LRT (red dots,

offset by +6 days) along with the vertical error bars representing the standard deviations.
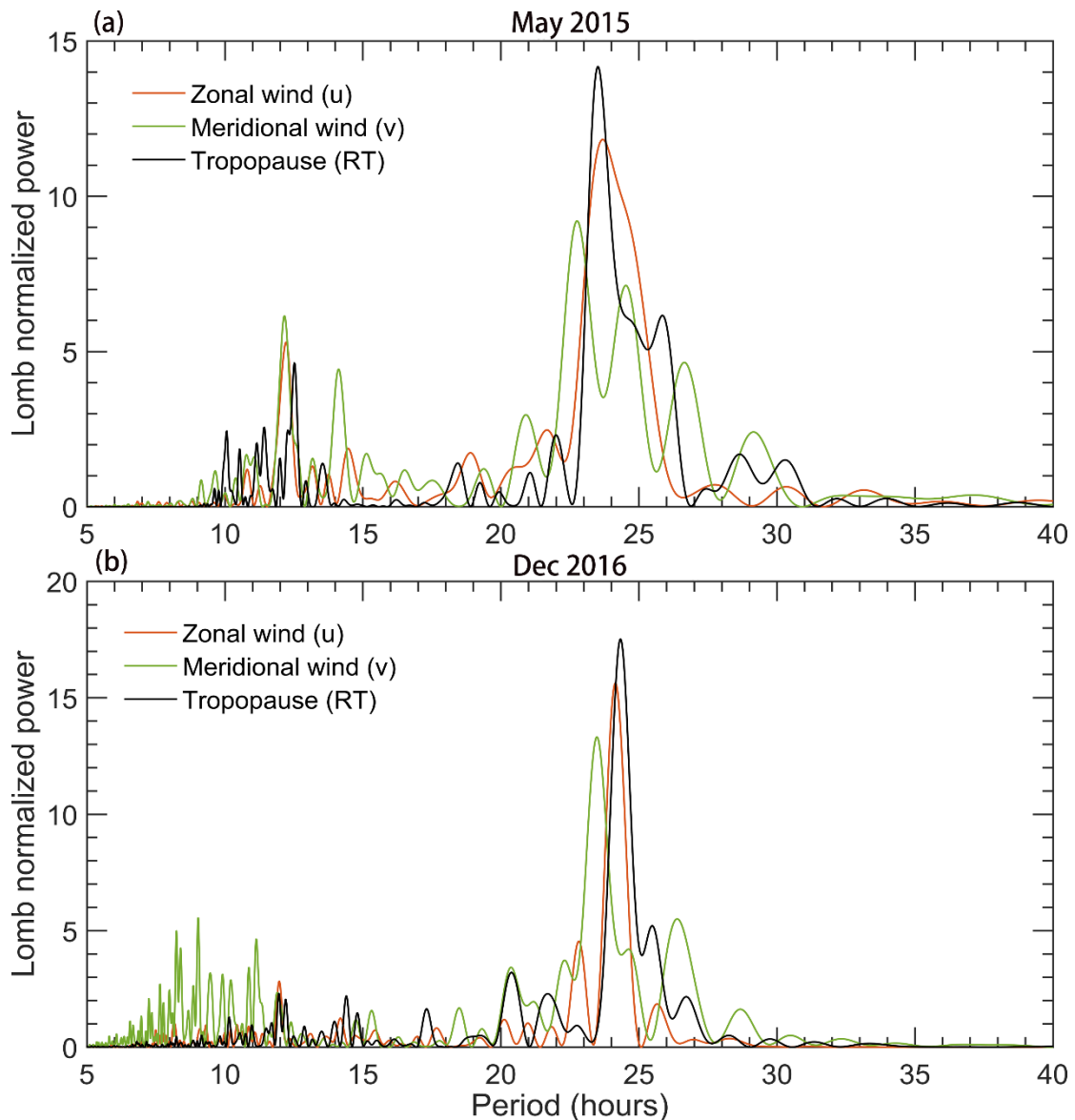
606

Figure 10. Lomb-Scargle periodograms of the RT height, zonal, and meridional wind

608   oscillations for specific months of (a) May 2015 and (b) December 2016. The zonal and

609   meridional wind for (a) is sampled at 9.85 km and (b) at 11 km.

610
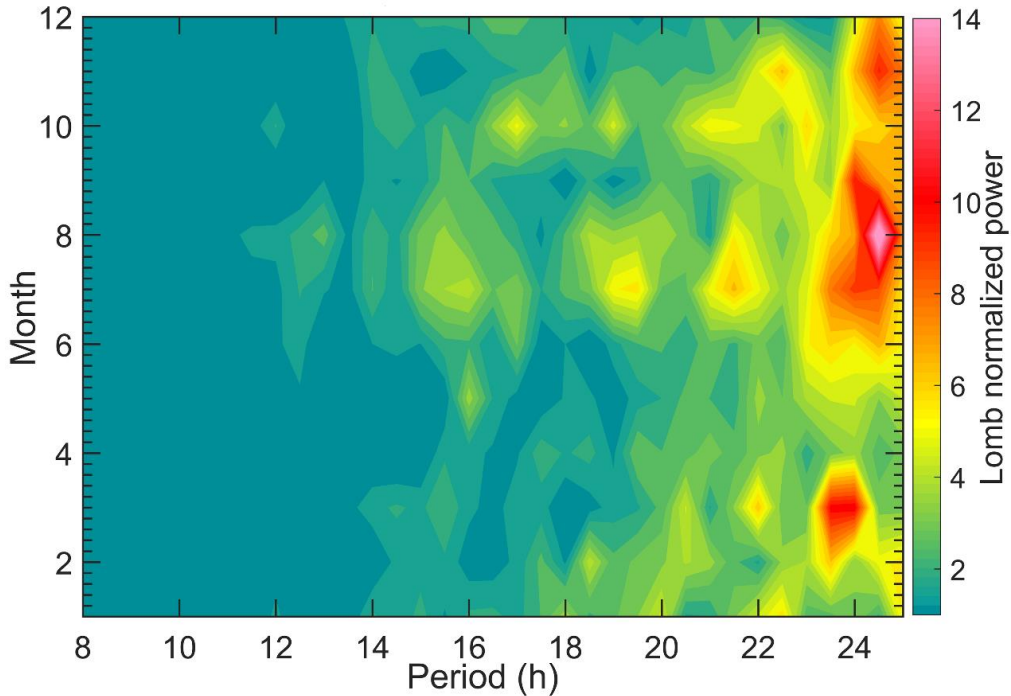
Figure 11. Mean Lomb-Scargle periodograms of RT height as a function of the time of

month during November 2011-May 2017.
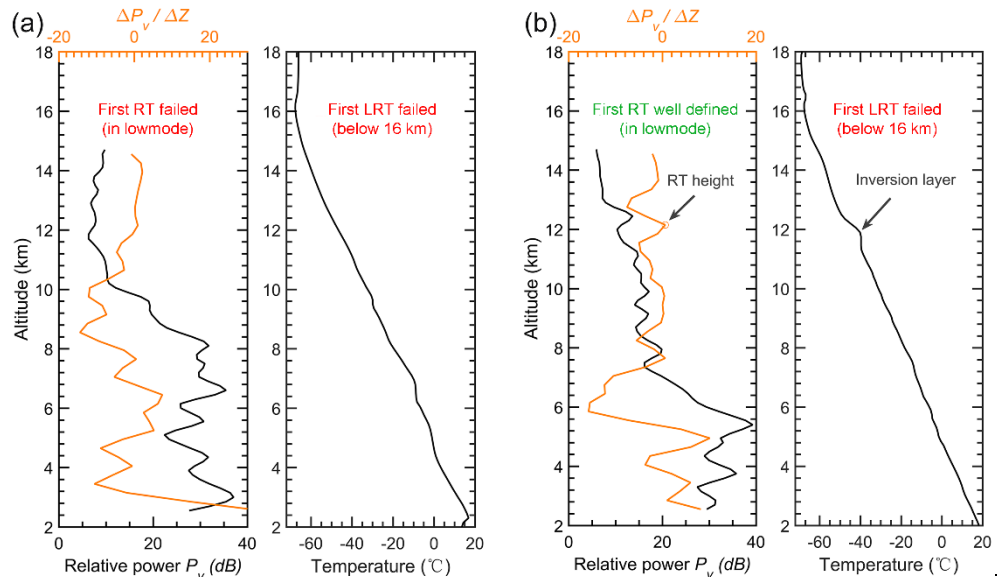
Figure 12. Example profiles of radar echo power and radiosonde temperature that (a)

both the RT and LRT definitions fail due to the continuing decrease in temperature on

00 UTC 7 July 2012 and (b) the temperature inversion layer failed to meet the LRT

definition but well defined in RT definition on 12 UTC 02 August 2012. Please note

that we only consider the conditions below 16 km.